POLITECNICO DI TORINO
Repository ISTITUZIONALE

Nonlinear dynamics of a 3D-printed pre-compressed beam structure: an experimental investigation

Original
Nonlinear dynamics of a 3D-printed pre-compressed beam structure: an experimental investigation / Anastasio, D., Daga, A.P., Fasana, A., Garibaldi, L., Marchesiello, S., Cheng, P.. - In: JOURNAL OF PHYSICS. CONFERENCE SERIES. - ISSN 1742-6588. - ELETTRONICO. - 2647:(2024), pp. 1-11. (XII International Conference on Structural Dynamics, Eurodyn 2023 Delft (NLD) 03/07/2023 - 05/07/2023) [10.1088/1742-6596/2647/9/092004].

Availability:
This version is available at: 11583/2990073 since: 2024-07-01T13:31:30Z

Publisher:
IOP Publishing

Published
DOI:10.1088/1742-6596/2647/9/092004

Terms of use:

This article is made available under terms and conditions as specified in the corresponding bibliographic description in the repository

Publisher copyright

(Article begins on next page)

10 September 2026

Journal of Physics: Conference Series

PAPER • **OPEN ACCESS**

Nonlinear dynamics of a 3D-printed pre-compressed beam structure: an experimental investigation

To cite this article: D Anastasio *et al* 2024 *J. Phys.: Conf. Ser.* **2647** 092004

View the article online for updates and enhancements.

You may also like

- Effects of incident energy and angle on carbon cluster ions implantation on silicon substrate: a molecular dynamics study
Ye Wei, Shengbo Sang, Bing Zhou et al.
- Perfect *DD** Molecular Prediction Matching the T_{cc} Observation at LHCb
Ning Li, Zhi-Feng Sun, Xiang Liu et al.
- Synthesis of two-dimensional/one-dimensional heterostructures with tunable width
Di Wang, Zucheng Zhang, Bo Li et al.

This content was downloaded from IP address 130.192.23.198 on 01/07/2024 at 14:21

Journal of Physics: Conference Series **2647** (2024) 092004 doi:10.1088/1742-6596/2647/9/092004

Nonlinear dynamics of a 3D-printed pre-compressed beam structure: an experimental investigation

D Anastasio*, A P Daga, A Fasana, L Garibaldi, S Marchesiello and P Cheng

Politecnico di Torino, Dipartimento di Ingegneria Meccanica ed Aerospaziale

*dario.anastasio@polito.it

Abstract. Engineering applications have conventionally aimed to avoid phenomena related to mechanical instabilities or buckling, as they can bring undesired nonlinear effects or even failure. In recent years however the research in this field has experienced an inversion of direction making use of such phenomena to improve the performance of solids and structures. In this context, the adoption of pre-compressed slender beam elements is one of the most common solutions. A typical application is the development of quasi-zero stiffness (QZS) vibration isolators, that bring a high static stiffness and an extremely low dynamic stiffness. As a general rule, the QZS characteristics can be obtained by coupling a negative stiffness effect with a positive one. When considering beam elements, the application of a compressive axial force can lead to a mechanical instability and to a negative stiffness region in the force-displacement characteristics. This paper studies the dynamical behaviour of such elements by comparing experimental measurements with a mathematical model. To this end, a 3D-printed V-shaped structure is considered, comprising two pre-compressed beam elements and a controllable pre-load. The regulation of the pre-load allows the V-structure to undergo tensile or compressive forces, thus altering its characteristics. In particular, the restoring force of the system can show regions of negative or quasi-zero stiffness when compressive forces are applied. The system is excited with an electromagnetic shaker considering different pre-loads, and the nonlinear dynamic behaviour is estimated from the measured responses. A comparison between experimental measurements and model predictions is eventually carried out to strengthen the understanding of the observed dynamical phenomena.

1. Introduction

The use of nonlinear elastic elements in dynamical systems has been widely explored in the past decades for performance improvements and vibration control. Practically, a nonlinear force-deflection curve can be obtained with a variety of configurations, such as combination of springs [1] and pre-stressed beams [2]. The latter case has been widely studied due to its simplicity [3], and can generate either hardening effects in the case of tensile forces [4,5] or softening effects in the case of compressive ones [6,7]. This often leads to negative or quasi-zero stiffness (QZS) regions, that can be exploited to obtain effective vibration isolators [8–11]. The design of devices to obtain a static QZS force-deflection curve has been studied in [1], while in [7,12] a double-well Duffing oscillator with a negative stiffness region has been characterized experimentally. Recently, pre-compressed beam structures obtained via 3D printing have been proposed [2,13] to achieve the negative stiffness behaviour.

Content from this work may be used under the terms of the Creative Commons Attribution 4.0 licence. Any further distribution of this work must maintain attribution to the author(s) and the title of the work, journal citation and DOI.
Published under licence by IOP Publishing Ltd

The presence of a negative stiffness region in the device force-deflection curve has important consequences in its dynamical behaviour. Not only the dynamical behaviour is geometrically nonlinear, but periodic oscillations can evolve to period doubling cascades and chaotic motion under external excitation [14,15] due to the presence of multiple stable and unstable equilibrium positions.

In this work, a 3D-printed pre-compressed beam structure is investigated to study its dynamical behavior. To this end, a V-shaped structure is considered, comprising two pre-compressed beam elements and a controllable pre-load. The regulation of the pre-load allows the V-structure to undergo tensile or compressive forces, thus altering its characteristics. In particular, the restoring force of the system can show regions of negative or quasi-zero stiffness when compressive forces are applied. A simplified quasi-static analytical model is proposed and compared with finite element (FE) simulations and quasi-static experimental tests. Then, the system is excited with an electromagnetic shaker considering different pre-loads, and the nonlinear dynamic behavior is estimated from the measured responses. A comparison between experimental measurements and model predictions is eventually carried out to strengthen the understanding of the observed dynamical phenomena.

2. V-shaped beam structure: design, models and quasi-static characterization

The system under test is a V-shaped beam structure as in **Figure 1**a. The structure is composed by two thin beams with thickness t in the form of a "V" with angle α. In the undeformed configuration, the distance between lower and upper surfaces is h_0 and the system is symmetric. When a preload distance d is applied to the lower surface, the structure deforms as in **Figure 1**b, and the new height is called h_p. The upper surface is free to slide along the x-axis and its coordinate is called z.

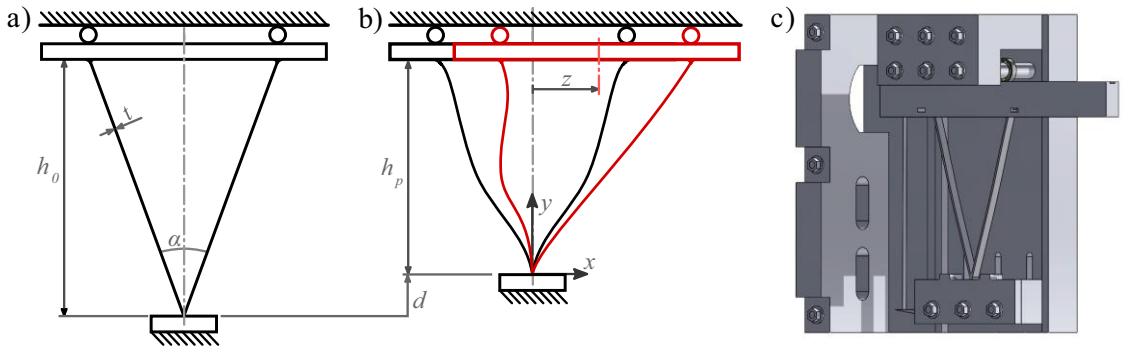

Figure 1. Scheme of the V-shaped structure. a) Undeformed configuration; b) Deformed configuration; c) Render.

The render of the device is shown in **Figure 1**c and the characteristic dimensions are listed in **Table 1**. A modular design has been chosen for the assembly, so that different V-shaped elements can be easily switched. The preload distance can be regulated continuously, while rolling bearings are used on the upper surface to guide the z motion.

Table 1. Dimensions and material properties.

Undeformed height h_0	97 mm
Thickness t	1 mm
Angle α	35 °
Filament material	PolyLactic Acid (PLA)

2.1. Simplified quasi-static model

Based on the V-shaped negative stiffness structure object of this study, a novel fully-analytical quasi-static simplified model is proposed. The model is based on a *m*-dof approximation of the continuum system to explain eulerian instability (i.e., buckling) in essential terms. The two beams of length L_0 are considered to be composed by N rigid bar-elements of size $\Delta L = L_0/N$ while the elasticity is concentrated at the elemental connections. Rotational springs of given torsional stiffnesses k_i (with $i = 1 \div N + 1$) are placed at the boundary of each element, whose orientation is ruled by its tilt angle θ_i measured starting from the initial angle $\alpha/2$. Given the free body reported in **Figure 2**, this lumped stiffness model implies N rotational equilibrium equations of the kind:

$$k_{i+1}(\theta_{i+1} - \theta_i) + k_i(\theta_i - \theta_{i-1}) + V\,\Delta L\,\sin\left(\theta_i + \frac{\alpha}{2}\right) - F\,\Delta L\,\cos\left(\theta_i + \frac{\alpha}{2}\right) = 0 \tag{1}$$

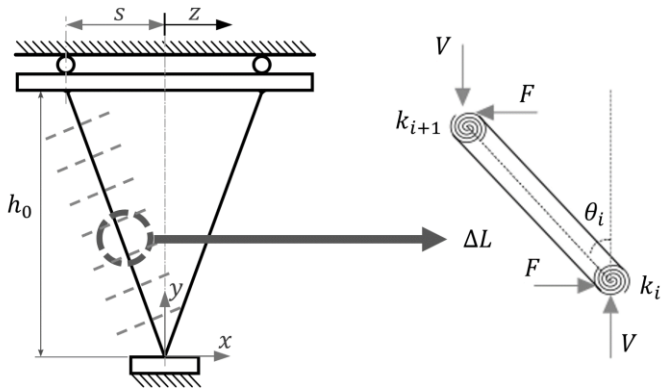

Figure 2. Simplified analytical model.

As a quasi-static solution is sought, the mass and inertia of the rigid elements can be neglected, leading to N unknowns θ_i plus two unknown forces F (along *x*) and V (along *y*), common to all the elements. These $N + 2$ unknowns can be derived as a function of the input displacement along *x* and *y* axes. Hence, a solution for the left beam can only be found by adding two geometrical constrains to the set of non-linear equations:

$$\sum_{i=1}^{N} \Delta L \cos\left(\theta_i + \frac{\alpha}{2}\right) = h_0 - d, \quad \sum_{i=1}^{N} \Delta L \sin\left(\theta_i + \frac{\alpha}{2}\right) = s + z \tag{2}$$

An analogous solution can be found for the right beam, so that the final forces $\mathcal{F}$ (along *x*) and $\mathcal{V}$ (along *y*) are derived for the whole V-shaped structure.

2.2. FE model

A finite element model is built in Ansys [16] for the V-shaped element. Figure 3 shows the static simulation when a compressive load (**Figure 3**a) and an imposed displacement along x (**Figure 3**b) are applied.

The *x*-direction and *y*-direction restoring forces $\mathcal{F}$ and $\mathcal{V}$ can eventually be extracted from the FE simulation and compared with the analytical predictions and the experimental observations. This paper will only focus on the *x*-direction restoring force $\mathcal{F}$ in the following.

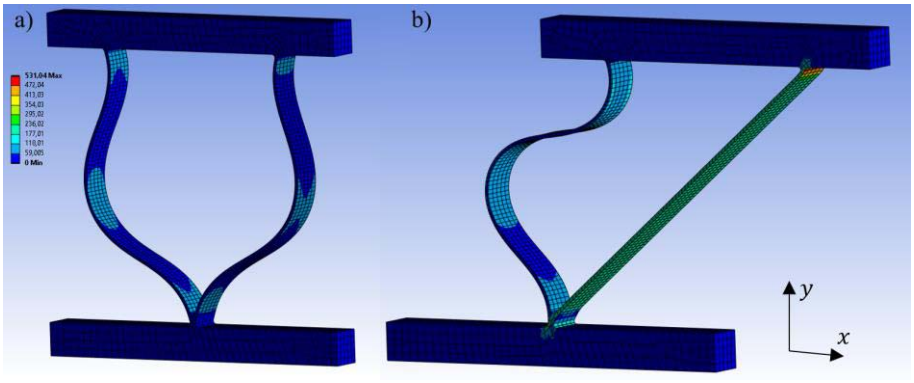

Figure 3. FE model. a) V-shaped structure under compression load; b) V-shaped structure under compression load and imposed displacement.

2.3. Device realization with 3D-printing technology

The use of 3D-printed parts allows for a rapid prototyping of the device at fairly low cost. The Ultimaker 3 Extended 3D-printer is used with generic PolyLactic Acid (PLA) filament. The printing parameters such as printing speed, in-fill values and wall thickness have been customized to accomplish the desired results in terms of accuracy. The sliding setup process for the V-shaped elements is shown in **Figure 4**a, while some printed samples are shown in **Figure 4**b.

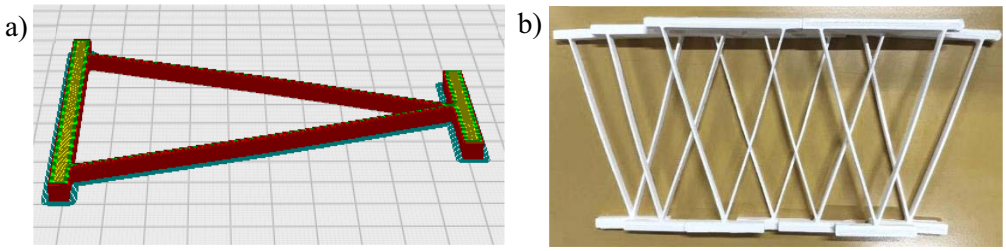

Figure 4. Sliding setup process of the V-shaped element in (a); printed samples in (b).

2.4. Quasi-static characterization

The device is first tested on an electromechanical tensile test bench (MTS QTEST Elite) to evaluate its quasi-static force-deflection curve. Tests are conducted with a strain rate of 15 mm/min and gravity is not accounted for. A photo of the experimental setup is depicted in **Figure 5**a and the experimental force-deflection curve $\mathcal{F}(z)$ is shown in **Figure 5**b as dashed-dotted lines. In particular, the blue colour refers to the preload distance $d = 5\ mm$ and the red color refers to the preload distance $d = 10\ mm$. In both cases, fluctuations are clearly visible in the negative stiffness region, that are likely to be related to sliding friction between the moving surface and the bearings. The experimental data is interpolated with a 9th order polynomial for the two preload distances and the results are plotted in **Figure 5**b as continuous lines with the same colour scheme. A negative slope is observed in both cases around the zero-position. The potential of the system $\mathcal{U}(z)$ can be computed as the integral of the restoring force $\mathcal{F}(z)$ and it is depicted in **Figure 5**c. As expected, it exhibits a double-well behavior with two local minima corresponding to the two stable equilibrium positions z_-^* and z_+^*, and a local maximum z_0^* corresponding to the central unstable equilibrium. The oscillations of the system are therefore said to be *in-well* when bounded around one equilibrium position, and *cross-well* when encompassing multiple equilibria.

A comparison with the predicted behavior obtained using the analytical (Section 2.1) and FE (Section 2.2) models is depicted in **Figure 6**a for $d = 5\ mm$ and in **Figure 6**b for $d = 10\ mm$. It can be observed how the general trend is preserved, although the negative stiffness slope predicted by the models is higher than the experimental one. The reason is twofold: *i)* the material properties of the

PLA filaments are deeply affected by the printing process and must be updated in the models; *ii)* the assumptions on the boundary conditions of the models may differ from the real case due to uncertainties and tolerances. Furthermore, a distinctive asymmetry can be noted in the experimental characteristics that is not present in the modelled setup, suggesting that a certain discrepancy exists between the two beams of the V-shaped element.

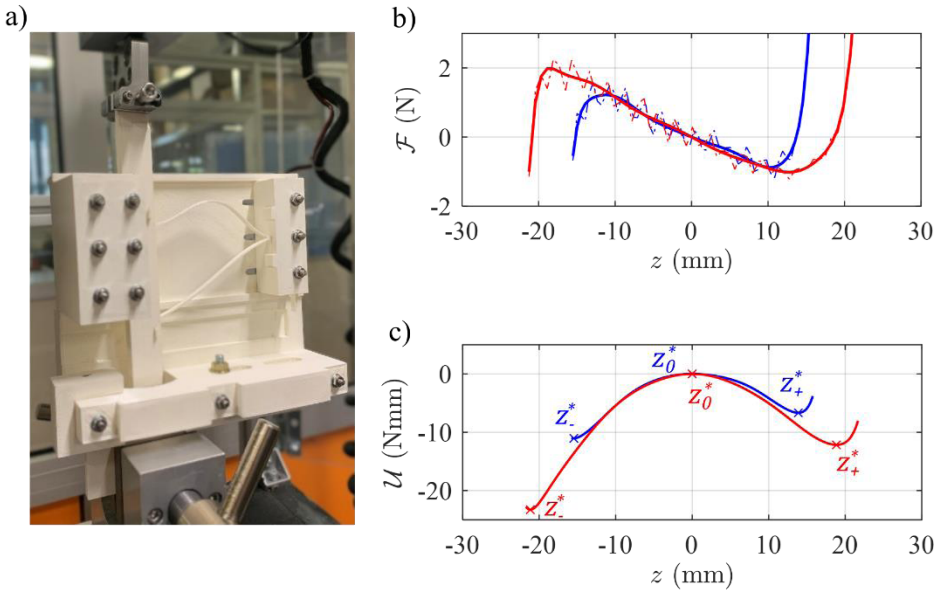

Figure 5. Quasi-static characterization. a) Photo of the experimental setup; b) Restoring force for *d=5mm* (in blue) and *d=10mm* (in red); c) Potential for *d=5mm* (in blue) and *d=10mm* (in red).

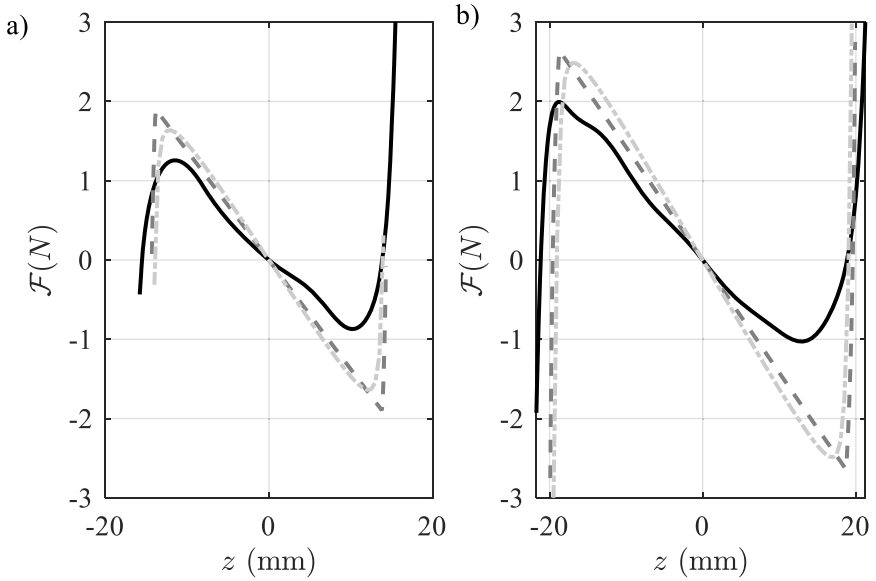

Figure 6. Quasi-static characterization. Black line: experimental characteristics; dashed dark-grey line: analytical model; dashed-dotted light-grey line: FE characteristics. a) *d=5mm*; b) *d=10mm.*

3. Experimental dynamic behaviour

The device is attached to an electromagnetic shaking table so that a displacement $b(t)$ can be imposed to the structure. The sliding mass is instrumented with an accelerometer to measure its absolute vertical acceleration $\ddot{y}(t)$, and the base acceleration $\ddot{b}(t)$ is measured with a second accelerometer. The system is excited with different excitation inputs and signals are sampled with a sampling frequency of 2048 Hz. A picture of the experimental setup in the zero-position is shown in **Figure 7**.

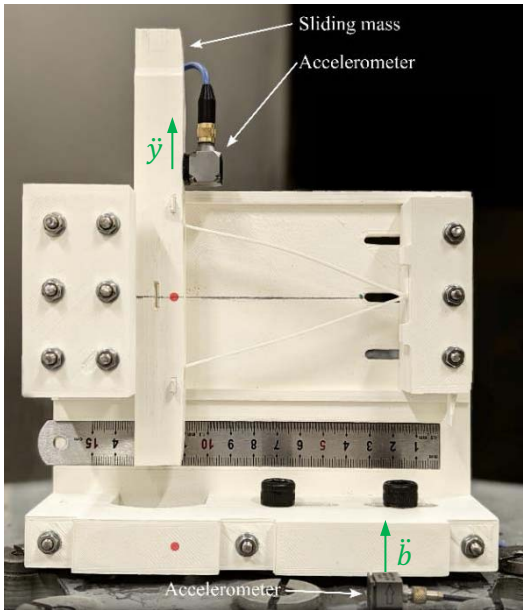

Figure 7. Experimental setup.

The two red dots visible in **Figure 7** correspond to two markers used together with a camera system to extract their displacement from the video using digital image correlation with a rate of 960 fps and a HD resolution [17].

First, the system is driven through two levels of random excitation around the equilibrium position z_{-}^{*} and with $d = 10\,mm$. Gaussian white noise is generated within the frequency range [5 100] Hz and the signals are recorded for 200 seconds. The RMS values of the base acceleration for the two excitation levels are 24 ms^{-2} (low-level) and 48 ms^{-2} (high-level). The transmissibility between the relative acceleration $\ddot{z} = \ddot{y} - \ddot{b}$ and the base acceleration $\ddot{b}$ can be computed using the H1-estimator and it is depicted in **Figure 8** in terms of its modulus $|T|$.

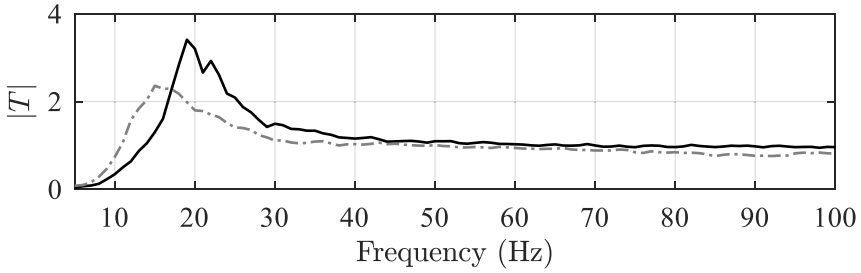

Figure 8. Transmissibility of the system, in-well oscillations around z_{-}^{*}. Continuous black line: low-level, 24 ms^{-2} RMS; dashed-dotted grey line: high-level, 48 ms^{-2} RMS.

An in-well resonance peak can be spotted between 15 and 20 Hz, and it can be seen how it shifts towards lower values when increasing the excitation level. This is symptomatic of a softening effect and it is coherent with the bi-stable nature of the device, as demonstrated by previous studies [7,15]. To investigate the dynamic behavior around the in-well resonance, a second set of tests is performed by driving the system with a linear sine-sweep excitation. The sweep starts at 14 Hz and ends at 24 Hz with a rate of 0.05 Hz/s. Two levels of excitation are considered and the in-well responses are measured around the negative (**Figure 9**a) and positive (**Figure 9**b) equilibrium positions. A clear jump-up phenomenon is observed, whose frequency depends on the excitation level. In particular, the jump frequency decreases for increasing excitation level, coherently with the previous findings.

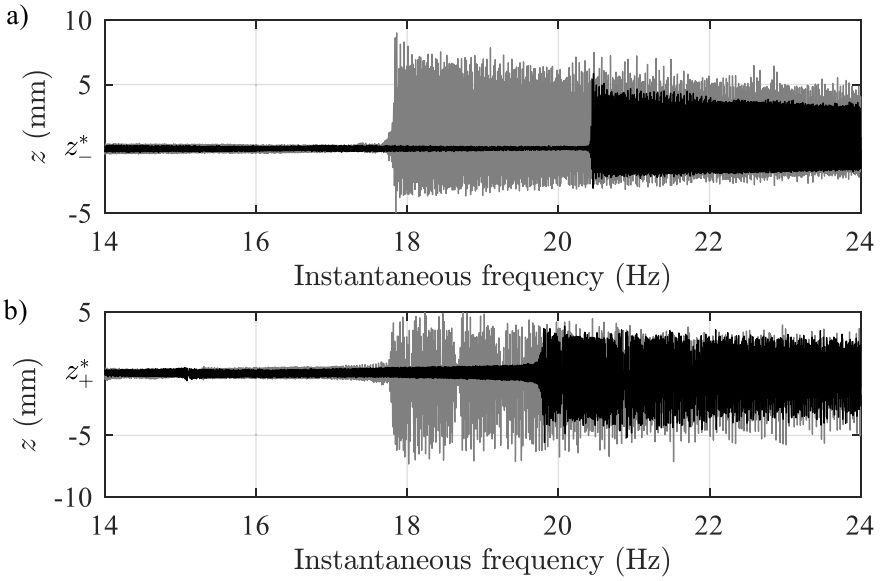

Figure 9. Sine-sweep excitation. Black line: low-level; grey line: high-level. a) In-well oscillations around z_-^*; b) In-well oscillations around z_+^*.

Eventually, a third set of tests is conducted by measuring the in-well response around z_-^* to a harmonic excitation at $\nu = 20\ Hz$ and for two excitation levels. The excitation level is referred to as the amplitude of the base motion b_0, equal to 0.5 mm in the first case (**Figure 10**a, b, c) and to 1.05 mm in the second case (**Figure 10**d, e, f). Super-harmonics of the exciting frequency (i.e. $2\nu, 3\nu, ...$) can be seen in the power spectral density (PSD) for the lowest excitation level case (**Figure 10**b). The phase diagram (**Figure 10**c) shows in this case a *period-1* solution. The highest excitation level causes the system to respond with a *period-2* solution instead, meaning that the output is periodic with twice the period of the input. This is visible in the sub-harmonics of the PSD (**Figure 10**e) and in the nested orbits of phase diagram (**Figure 10**f). The period-doubling phenomenon is characteristic of several classes of nonlinear systems. In case of systems with a double-well potential, it is generally the principle of a period doubling cascade that can lead to a cross-well motion [14,15].

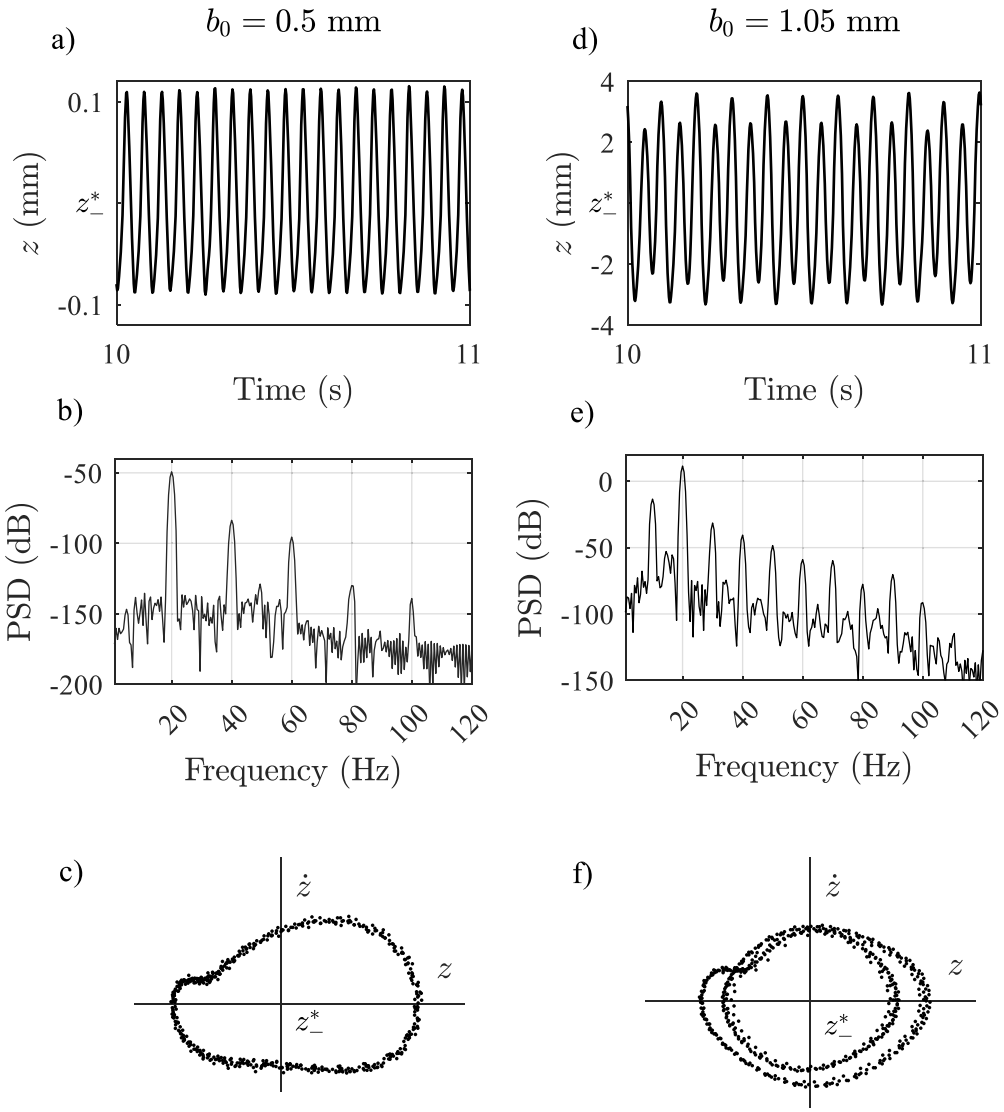

Figure 10. Harmonic tests at 20 Hz: one-second time plot, power spectral density and phase plane. Base amplitude of 0.5 mm in (a), (b), (c); base amplitude of 1.05 mm in (d), (e), (f).

Assuming that the equivalent inertia of the moving parts can be concentrated on the sliding mass, the dynamic equation of motion of the relative motion $z(t) = y(t) - b(t)$ can be written treating the system as a single-degree-of-freedom system:

$$m\ddot{z} + \mathcal{R}(z, \dot{z}) = -m\ddot{b}, \tag{3}$$

where $\mathcal{R}(z, \dot{z})$ is the restoring surface. This is the sum of the restoring force $\mathcal{F}(z)$ and of the dissipative force $\mathcal{D}(z, \dot{z})$ that can generally be written as a function of both displacement and velocity. It is not the purpose of this paper to properly estimate the dissipative force and the reader can refer to [7,12] for the experimental estimation of $\mathcal{D}$ in a bi-stable system with a similar restoring force. It can be stated, however, that the main source of dissipation comes from friction between the sliding surfaces.

An estimation of the restoring force $\mathcal{F}(z)$ can be obtained from the dynamic tests by applying the Restoring Force Surface (RFS) method [18,19]. This is done by slicing the experimental restoring

surface around the zero-velocity region, where the damping force is assumed to be negligible with respect to the restoring force. The application of the RFS method to the high-level sine-sweep tests of **Figure 9** gives the points depicted in red in **Figure 11**. A good overlapping between the red points and the quasi-static experimental measurement can be observed, confirming the previous findings.

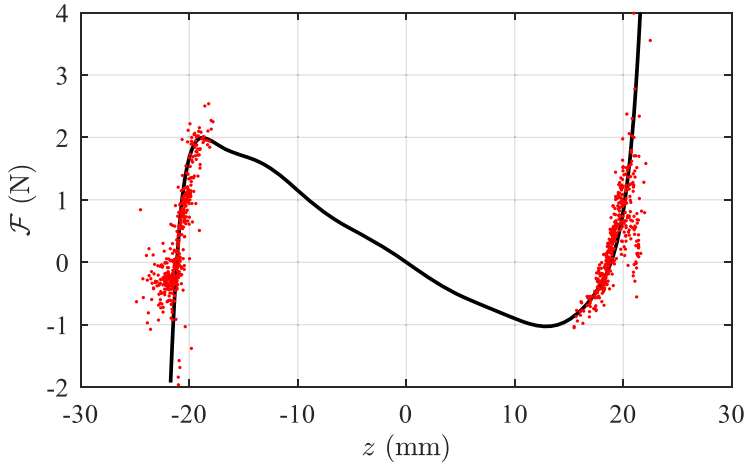

Figure 11. Estimation of the restoring force from the dynamic tests. Red dots: RFS method. Black line: quasi-static experimental characterization.

4. Conclusions

This paper studied the dynamical behavior of a 3D-printed pre-compressed beam structure. To this end, a 3D-printed V-shaped structure has been considered, comprising two pre-compressed beam elements and a controllable pre-load. The regulation of the pre-load allows the V-structure to undergo tensile or compressive forces, thus altering its characteristics. In particular, the restoring force of the system can show regions of negative or quasi-zero stiffness when compressive forces are applied. A simplified quasi-static analytical model has been proposed and compared with finite element simulations and quasi-static experimental tests. Then, a series of dynamic tests has been performed with different pre-loads and excitation types, with the observation of period doubling phenomena. A comparison between experimental measurements and model predictions is eventually carried out to strengthen the understanding of the observed phenomena. Future work may include dynamic tests involving cross-well motion and a dedicated study about the estimation of the damping force.

References

[1] Gatti G, Shaw A D, Gonçalves P J P and Brennan M J 2022 On the detailed design of a quasi-zero stiffness device to assist in the realisation of a translational Lanchester damper *Mech. Syst. Signal Process.* **164**

[2] Kuppens P R, Bessa M A, Herder J L and Hopkins J B 2021 Monolithic binary stiffness building blocks for mechanical digital machines *Extreme Mech. Lett.* **42** 101120

[3] Gatti G, Brennan M J and Tang B 2019 Some diverse examples of exploiting the beneficial effects of geometric stiffness nonlinearity *Mech. Syst. Signal Process.* **125** 4–20

[4] Anastasio D, Marchesiello S, Kerschen G and Noël J P 2019 Experimental identification of distributed nonlinearities in the modal domain *J. Sound Vib.* **458** 426–44

[5] Claeys M, Sinou J J, Lambelin J P and Alcoverro B 2014 Multi-harmonic measurements and numerical simulations of nonlinear vibrations of a beam with non-ideal boundary conditions *Commun. Nonlinear Sci. Numer. Simul.* **19** 4196–212

[6] Seunghoon P and Dooyoung H 2008 Pre-shaped buckled-beam actuators: Theory and experiments *Sens. Actuators Phys.* **148** 186–92

[7] Zhu R, Marchesiello S, Anastasio D, Jiang D and Fei Q 2022 Nonlinear system identification of a double-well Duffing oscillator with position-dependent friction *Nonlinear Dyn.* **108** 2993–3008

[8] Lee C M, Goverdovskiy V N and Temnikov A I 2007 Design of springs with "negative" stiffness to improve vehicle driver vibration isolation *J. Sound Vib.* **302** 865–74

[9] Le T D and Ahn K K 2011 A vibration isolation system in low frequency excitation region using negative stiffness structure for vehicle seat *J. Sound Vib.* **330** 6311–35

[10] Antoniadis I, Chronopoulos D, Spitas V and Koulocheris D 2015 Hyper-damping properties of a stiff and stable linear oscillator with a negative stiffness element *J. Sound Vib.* **346** 37–52

[11] Salvatore A, Carboni B and Lacarbonara W 2022 Nonlinear dynamic response of an isolation system with superelastic hysteresis and negative stiffness *Nonlinear Dyn.* **107** 1765–90

[12] Anastasio D and Marchesiello S 2020 Experimental Characterization of Friction in a Negative Stiffness Nonlinear Oscillator *Vibration* **3** 132–48

[13] Kuppens P R, Bessa M A, Herder J L and Hopkins J B 2021 Compliant Mechanisms That Use Static Balancing to Achieve Dramatically Different States of Stiffness *J. Mech. Robot.* **13** 021010

[14] Strogatz S H 1994 *Nonlinear dynamics and Chaos: with applications to physics, biology, chemistry, and engineering* (Addison-Wesley Pub)

[15] Kovacic I and Brennan M J 2011 *The Duffing equation : nonlinear oscillators and their phenomena* (Wiley)

[16] ANSYS Workbench 2022 R2, ANSYS Inc.

[17] André H, Leclère Q, Anastasio D, Benaïcha Y, Billon K, Birem M, Bonnardot F, Chin Z Y, Combet F, Daems P J, Daga A P, Geest R D, Elyousfi B, Griffaton J, Gryllias K, Hawwari Y, Helsen J, Lacaze F, Laroche L, Li X, Liu C, Mauricio A, Melot A, Ompusunggu A, Paillot G, Passos S, Peeters C, Perez M, Qi J, Sierra-Alonso E F, Smith W A and Thomas X 2021 Using a smartphone camera to analyse rotating and vibrating systems: Feedback on the SURVISHNO 2019 contest *Mech. Syst. Signal Process.* **154**

[18] Masri S F and Caughey T K 1979 *A Nonparametric Identification Technique for Nonlinear Dynamic Problems*

[19] Dossogne T, Masset L, Peeters B and Noël J P 2019 Nonlinear dynamic model upgrading and updating using sine-sweep vibration data *Proc. R. Soc. Math. Phys. Eng. Sci.* **475** 20190166